Meteorology and Atmospheric Physics (2026) 138:7
https://doi.org/10.1007/s00703-025-01112-9

REVIEW ARTICLE

The evolution of the moisture flux with the onset and retreat isochrones of the Indian summer monsoon

Amarjeet[1,2] · Vasubandhu Misra[2,3] · Arun Chakraborty[1] · Anil Kumar Gupta[4]

Received: 17 May 2025 / Accepted: 9 December 2025

Abstract
The progression of the moisture flux with the seasonal evolution of the Indian summer monsoon (ISM), as followed by the evolution of its onset and retreat isochrones, is examined using European Reanalysis v5 (ERA5) and the India Meteorological Department rainfall analysis. In this study, the onset and retreat dates of the ISM rainfall diagnosed at the granularity of calendar days of the year are aggregated to a few homogeneous regions of India for which a detailed moisture flux analysis is conducted. Our analysis reveals that the early onset of summer rains in northeast India is unique from the rest of India, with its southerly moisture transport, which is mainly from the Bay of Bengal. The onset of the ISM in other regions is characterized by strong cross-equatorial southwesterly moisture flux. The retreat of the ISM shows a southward retreat of the moisture flux across the Indian Ocean. Interannual variations in the onset and withdrawal dates are closely linked to anomalies in cross-equatorial moisture transport, indicating that the southwestern Arabian Sea and northeastern Bay of Bengal may serve as key sentinel regions for upper-air monitoring of ISM variability. These areas exhibit significant fluctuations in both the non-divergent and irrotational components of moisture flux during onset, providing potential early indicators of anomalous monsoon evolution and would nicely complement existing seasonal monsoon prediction practices.

1 Introduction

The Indian summer monsoon (ISM) is a crucial driver of terrestrial convection, showcasing a strong seasonal cycle that plays a vital role in the atmospheric general circulation. The spectacular seasonal cycle of the ISM is characterized by abrupt changes in the daily rain rates (Ananthakrishnan and Soman 1988), changes in wind direction and speed (Ramage 1971), abrupt changes in the vertically integrated moisture flux (Fasullo and Webster 2003), changes in precipitable water (Zeng and Lu 2004), and meridional gradient of temperature (Yanai et al. 1992). Noska and Misra (2016) introduced an objective method for the diagnosis of the onset and retreat of the all-India monsoon onset, which was based on the inflection points in the daily cumulative anomaly curve of rainfall over India. By this definition, the onset date was diagnosed as the first day when the daily rain rate exceeded its annual mean climatology, while the retreat date was the last day in the year when the daily rain rate fell below the annual mean climatology. In a further extension of this work, Misra et al. (2018) used the same definition to define the onset and retreat dates of the ISM at the same granularity as the rainfall analysis. Noska and Misra (2016) showed that the diagnosis of these onset/retreat dates of the ISM coincided with the seasonal thermodynamic and dynamic changes in the monsoon circulation. For instance, the seasonality of the large-scale land-ocean thermal contrast and the meridional net heat transport in the upper tropical Indian Ocean was closely associated with the diagnosed onset and retreat dates of the ISM rainfall.

Trenberth et al. (2003) suggest that the rainfall process is not a very efficient process. They claim a large fraction of the moisture that is condensed as precipitation in an air column is sourced remotely through moisture flux

Communicating Editor: Silvia Trini-Castelli.

✉ Amarjeet
amar.vidyarthi@fsu.edu

[1] Centre for Ocean, River, Atmosphere, and Land Sciences (CORAL), Indian Institute of Technology Kharagpur, Kharagpur, India

[2] Center for Ocean-Atmospheric Prediction Studies, Florida State University, Tallahassee, FL, USA

[3] Department of Earth, Ocean and Atmospheric Science, Florida State University, Tallahassee, FL, USA

[4] Department of Geology and Geophysics, Indian Institute of Technology, Kharagpur, Kharagpur, India

Published online: 22 December 2025

convergence, while the contribution of local evaporation and precipitable water is relatively small. Similarly, Fasulo and Webster (2003) indicate that rainfall exceeds evaporation in terrestrial wet monsoonal regions, which serves as strong evidence that lateral transport of moisture is critical for the existence of monsoonal rains. Therefore, there is a strong interest in understanding the remote sources of moisture relating to their transport and advection in the large seasonal changes of the ISM (Clemens and Oglesby 1992; Ghosh et al. 1978; Levine and Turner 2011; Pisharoty 1965; Ratna et al. 2016). However, many of these earlier studies depend on atmospheric reanalysis products that have periodically been generated from updated models, observations, and assimilation techniques (Amarjeet et al. 2023; Misra et al. 2012; Patil et al. 2019; Sebastian et al. 2016; Shah and Mishra 2014; Sharma et al. 2024, 2025). For example, Misra et al. (2012) indicate that the terrestrial and oceanic sources of moisture to ISM are significantly different between the three reanalyses that they examined, which stem from differences in surface evaporation, low-level winds, and moisture in the air column. Similarly, Shah and Mishra (2014) show different biases in precipitation and temperature related to the ISM in three different reanalyses. Likewise, Sebastian et al. (2016) show that there is large uncertainty in the estimates of water availability computed as the difference between evaporation and precipitation over the South Asian land mass across different reanalyses. Some recent studies using numerical models and a Lagrangian approach for moisture trajectories showed that the nearby moisture sources play a vital role in the onset phase, while the far-distant sources are responsible for the moisture supply after the monsoon matures (Pathak et al. 2017; Volonté et al. 2020). Nevertheless, observational studies indicate the potential role of remote sources in moisture supply during the onset phase and deciding the pace of progression, as suggested by Yadav and Singh (2017), who suggest the role of intense cross-equatorial moisture supply in the timely onset and its faster progression across South Asia.

In this study, we intend to use European Reanalysis version 5 (ERA5; Hersbach et al. 2019), which is one of the most recently generated global atmospheric reanalyses. The principal objective of this study is to understand the seasonal characteristics of the moisture flux in relation to ISM in ERA5. The moisture flux is divided in this study between irrotational (divergent) and non-divergent (rotational) components, which represent the moisture source/sink regions and the water vapor transport components, respectively (Chakraborty et al. 2006). Krishanmurti et al. (1981) showed that the non-divergent component is the contributing part for the onset over a region by providing ample moisture supply by triggering convection, while the irrotational component indicates the source and sink of moisture. In this study, the moisture analysis is done with regard to the evolution of the ISM, which is characterized by the onset and retreat of the associated rainfall following Misra et al. (2018). The onset and retreat of the associated rainfall are pinned to calendar dates of the year at the granularity of the rainfall analysis, which is then aggregated to a few homogeneous regions (based on the homogeneity of onset/retreat dates) within India. The novelty of this study is the use of the objective definition of the onset and retreat dates of the ISM at each grid point following Misra et al. (2018) to ascertain the evolution of the atmospheric moisture over the ISM region. In the following section, we describe the data and methods used in this study, followed by the analysis of the results in Sect. 3. Conclusions are provided in Sect. 4.

2 Data and methods

We use the daily rainfall data from the India Meteorological Department (IMD) rain gauge analysis available at 0.25° grid resolution at daily intervals from 1901 to the present, following Pai et al. (2014, 2015). The climatology for the above-mentioned period is used to compute the onset and retreat dates as described in Misra et al. (2018). However, the diagnosis of onset/retreat dates for this study is done only for the period of 1980–2023. We also use ERA5 available at 0.25° grid spacing for the same period for upper air variables.

Using ERA5 datasets, the non-divergent (ψ) and irrotational (χ) components of the moisture flux are calculated following Chakraborty et al. (2006). We calculate the zonal (Q_u) and the meridional (Q_v) components of moisture flux as:

$$\mathrm{Q_u} = \frac{1}{g}\int_{P_t}^{P_s} qu\, dp \;\&\; \mathrm{Q_v} = \frac{1}{g}\int_{P_t}^{P_s} qv\, dp \tag{1}$$

where q is specific humidity; g is the acceleration due to gravity; u and v are zonal and meridional wind components, respectively; P_s, is the pressure at the bottom of the air column; P_t, pressure at the top of the air column. The moisture flux vector, $\mathbf{Q}$, can be written as:

$$\mathbf{Q} = \mathrm{Q_u}\hat{i} + \mathrm{Q_v}\hat{j} \tag{2}$$

$\mathbf{Q}$ is further decomposed into its non-divergent and irrotational components (Rosen et al. 1979) by writing in terms of stream function (ψ) and velocity potential (χ) as:

$$\mathbf{Q} = \hat{k} \times \nabla\psi + \nabla\chi \tag{3}$$

$$\nabla^2\psi = \hat{k}.\nabla \times \mathbf{Q} \tag{4}$$

$$\nabla^2\chi = \nabla.\mathbf{Q} \tag{5}$$

The non-divergent and irrotational components of moisture flux are calculated from Eqs. 4 and 5 using the spectral method (Krishnamurti et al., 2006). The irrotational ($\vec{Q}^d$) and non-divergent ($\vec{Q}^r$) moisture flux vectors are calculated from χ and ψ respectively, as:

$$\begin{aligned} Q_u^r &= -\frac{\partial\psi}{\partial y},\ Q_v^r = \frac{\partial\psi}{\partial x} \text{ and} \\ Q_u^d &= \frac{\partial\chi}{\partial x},\ Q_v^d = \frac{\partial\chi}{\partial y} \end{aligned} \tag{6}$$

The non-divergent component ($\boldsymbol{Q}^r$) represents moisture transport, while the irrotational component ($\boldsymbol{Q}^d$) emphasizes the source or sink region of the moisture. These vectors can be further decomposed into their scalar components as:

$$\boldsymbol{Q}^r = Q_u^r + Q_v^r \tag{7}$$

$$\boldsymbol{Q}^d = Q_u^d + Q_v^d \tag{8}$$

Homogeneous regions within India are identified based on the homogeneity of the climatological onset and retreat dates of the ISM separately.

The moisture flux vector, decomposed into its non-divergent component, provides information about the regions of atmospheric moisture supply, while the irrotational part shows the source and sink of moisture by way of its consumption or export from the related convective process (Amarjeet et al. 2025). In May/June, the onset of ISM depends upon several factors, of which moisture has its unique importance. The higher SSTs and steeper land-ocean pressure gradient result in the moisture supply to the Indian subcontinent, which we show using the non-divergent part of moisture flux, showing how it strengthens due to favorable conditions that help supply more moisture to the Indian subcontinent. In combination with thermodynamic factors, this results in the onset over a region. The irrotational part of the moisture flux, on the other hand, reflects the source of this moisture that is being supplied to a region at the time of the onset.

We investigate the moisture flux over different vertical atmospheric layers, which include the lower (1000–700 hPa) and middle (700–400 hPa) tropospheric layers. In atmospheric layers above 400 hPa, the moisture flux is comparatively much lower owing to the relative aridity in the layers.

The ERA5 dataset is also used to calculate large-scale atmospheric stability (γ_{ls}), as outlined by Cook and Seager (2013) as:

$$\gamma_{ls} = \delta_{surf} - \delta^*_{700} \tag{9}$$

Where, δ is the moist static energy (MSE) computed as

$$\delta = c_pT + gz + Lq \tag{10}$$

And δ_{surf} is the surface moist static energy computed with 2 m temperature and specific humidity, and δ^*_{700} is the saturated moist static energy at 700 hPa. According to Cook and Seager (2013), the difference in MSE between a rising parcel from the surface that becomes saturated at the lifting condensation level and the saturated MSE at a specific height in the atmosphere, typically above the boundary layer (~700 hPa), is directly linked to the parcel's thermal buoyancy at that altitude. When the moist static energy of a rising, saturated parcel exceeds the saturated moist static energy of the surrounding environment, the parcel experiences positive buoyancy. This leads to an unstable column, which in turn triggers convection and precipitation, as highlighted by Khairoutdinov and Randall (2006).

3 Results and discussion

a) Climatology

The climatological onset and retreat dates following Misra et al. (2018) are shown in Fig. 1. Each of the panels in Fig. 1a-d and e-g are binned at intervals of 30 days to be able to delineate distinct regions of spatially coherent, homogeneous regions of onset and retreat dates. For example, Fig. 1a, b, c, and d delineate the onset of the rainy season in the northeastern (Region I), Kerala-Karnataka-Gangetic-Brahmaputra basins (Region II), central-northwestern India (Region III), and Tamil Nadu-Jammu & Kashmir region (Region IV), which occur before May 10 (Julian day of 130), between May 11 and June 9 (Julian days between 131 and 160), between June 10 and July 9 (Julian days between 161 and 190), and after July 10 (after Julian day 191), respectively. The early onset of the ISM rains in northeastern India (Fig. 1a) is mentioned in several other previous studies (e.g., Misra et al., 2018; Zahan et al. 2021; Sharma et al. 2023; Saha et al. 2023; Das et al. 2024). Similarly, Fig. 1e, f, and g isolate the homogeneous regions based on retreat dates at intervals of 20 days of the rainy season over northwestern (Area I), central-northeastern (Area II), and peninsular India (Area III), respectively. The chronology of the retreat of ISM rains from Area I to II and then III is noted in several previous studies (e.g., Ramage

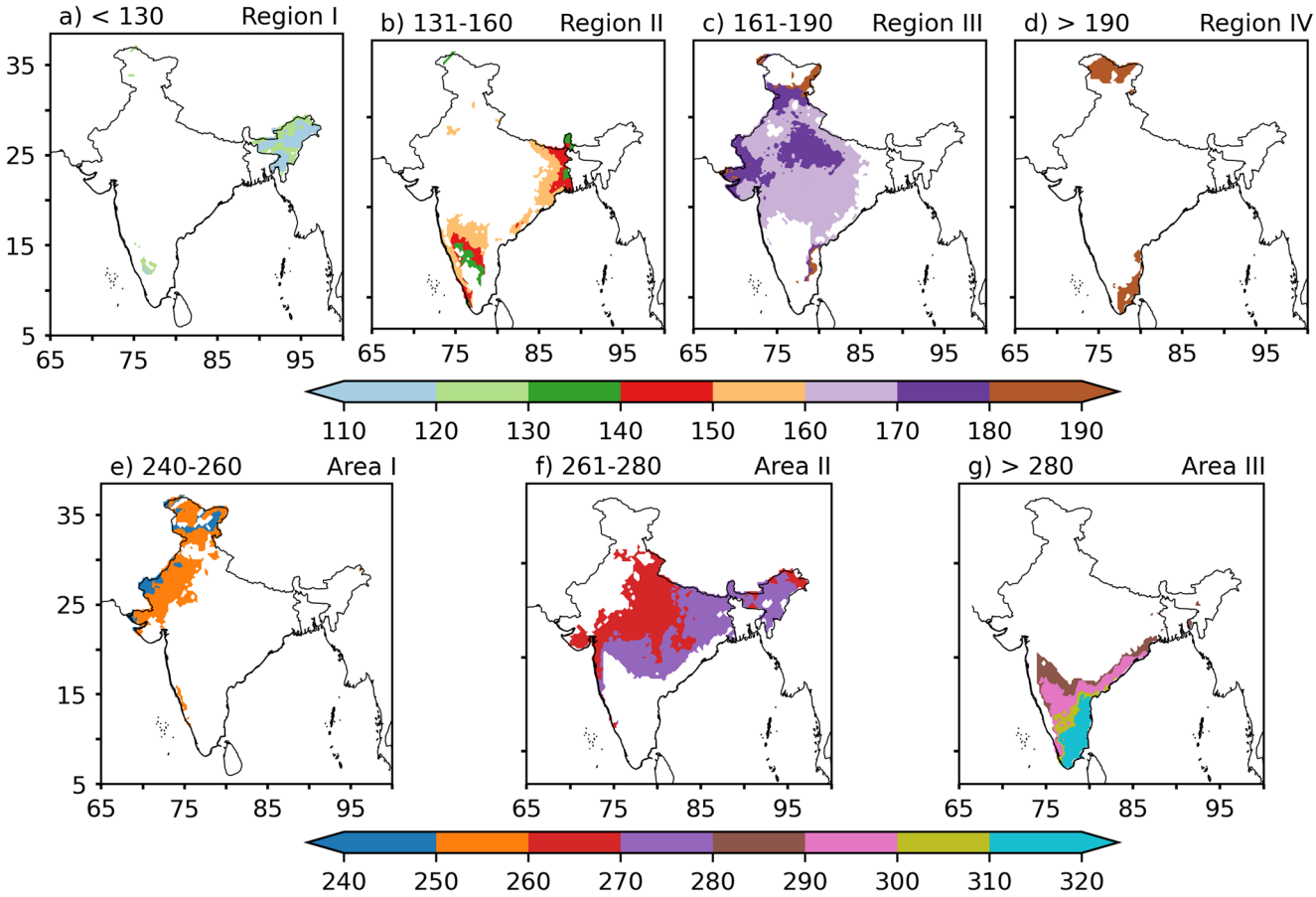

Fig. 1 The climatological (**a**-**d**) onset dates and (**e**-**g**) retreat dates of the ISM in Julian days from the gridded IMD rainfall data (Pai et al. 2014a, b). The shaded areas represent (**a**) Region I, (**b**) Region II, (**c**) Region III, (**d**) Region IV, (**e**) Area I, (**f**) Area II, and (**g**) Area III

1971; Ananthakrishnan and Soman 1988; Janowiak and Xie 2003). As noted in Misra et al. (2018), the granularity of the definition of the onset/retreat of the ISM rainfall offers a unique perspective on the discrete evolution of the ISM compared to other studies conducted with area-averaged onset/retreat indices (e.g., 'Kerala onset' of Ananthakrishnan et al. 1967). For instance, Misra et al. (2018) contend that the relation of the variations in the onset of the ISM rains in northeastern India to the onset over the rest of India is revealed because of the high-resolution definition of the onset/retreat dates of the ISM rainfall. Similarly, Misra and Bhardwaj (2020) reveal unique teleconnection patterns of variations in the length of the ISM season with ENSO from this definition of local onset/retreat of the ISM.

It may be noted that the spatially coherent regions for the onset and retreat dates are not the same, both in terms of their areas of coherency and the interval at which they are isolated. This reflects the asymmetry of the evolution of the ISM, which is indicated in earlier studies also (Krishnakumar and Lau 1998; Prasad and Hayashi 2005; Syroka and Toumi 2004).

The corresponding standard deviations of the onset dates in Fig. 2a show that the central and western coast of India has the least variability, while peninsular India, Jammu & Kashmir, and northeastern India exhibit large standard deviations. Similarly, variability of the retreat dates of the rainy season has a similar spatial pattern, with central India exhibiting the least variation, while peninsular India, Jammu & Kashmir, and northeastern India show large standard deviations. Interestingly, the variability of retreat dates is larger than the onset dates, as noted in earlier studies also (Misra et al., 2018; Noska and Misra 2016). In the rest of this study, we will use Regions I, II, and III for the analysis of the evolution of the ISM around the onset date and Areas I, II, and III for the analysis of the evolution of the ISM around the retreat dates. Region IV is neglected owing to the marginal precipitation received during the ISM.

The climatological non-divergent components of the vertically integrated (1000 to 200 hPa) moisture flux in mid to late April (which corresponds with onset dates over Region I) shows that the moisture flux over northeastern India is sustained by the southerly and westerly fluxes from the Bay of Bengal when the southwesterly flux over the Arabian Sea

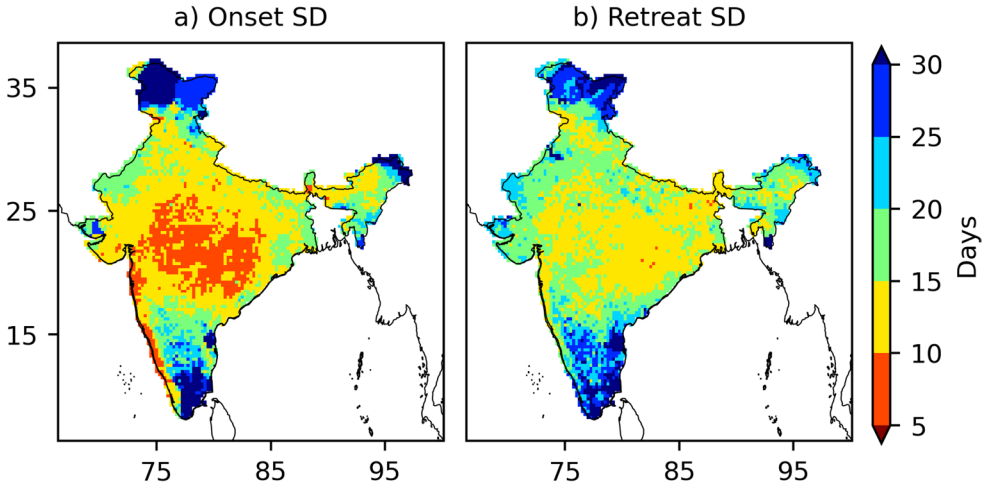

Fig. 2 The standard deviation (SD) of (**a**) onset dates and (**b**) retreat dates of the ISM in Julian days

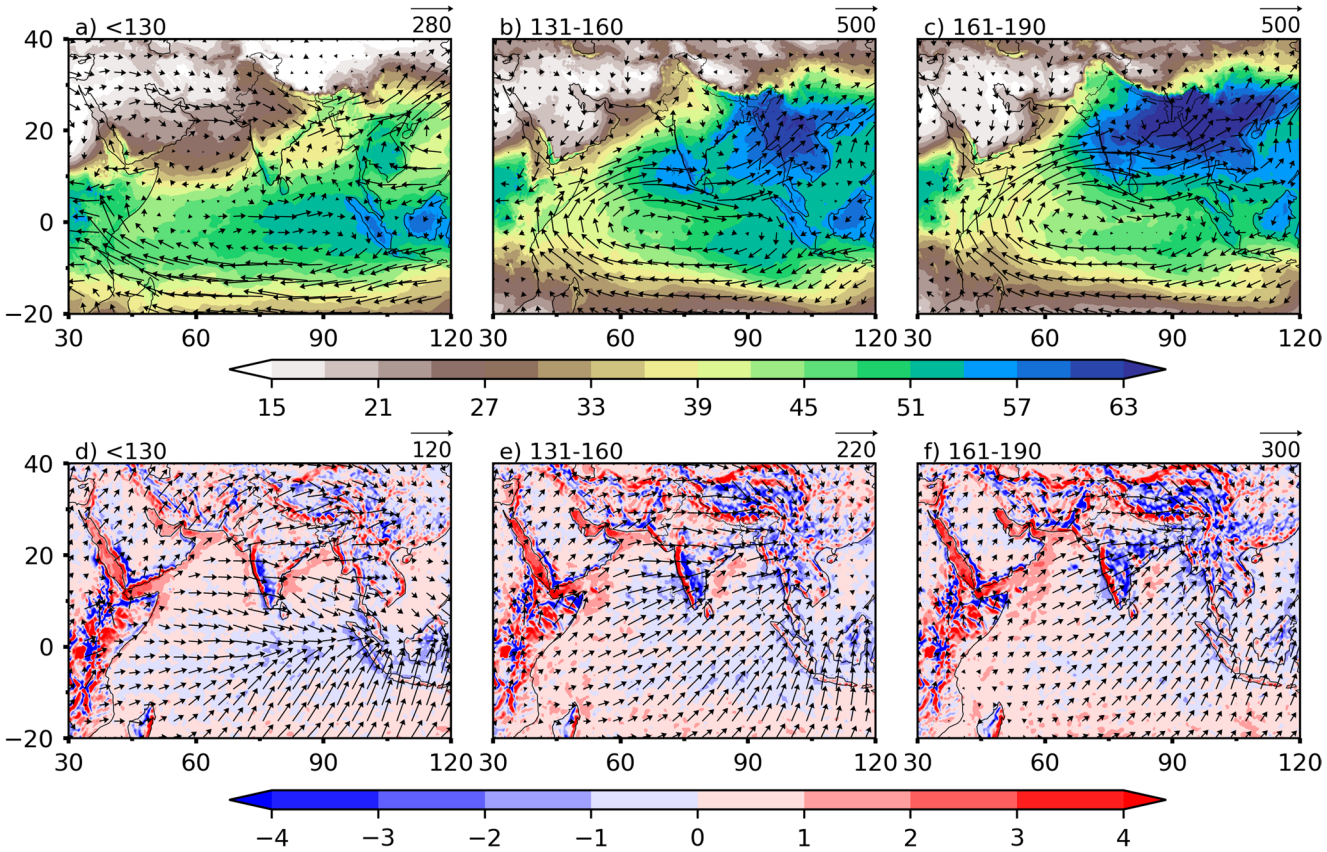

Fig. 3 The climatological mean of the (**a**, **b**, **c**) precipitable water (shaded; mm) non-divergent (Eq. 7 in text; vectors; $kgm^{-1}s^{-1}$) and (**d**, **e**, **f**) irrotational components of the vertically integrated (1000 to 200 hPa) moisture flux (Eq. 8 in text; vectors; $kgm^{-1}s^{-1}$) and divergence of moisture flux (Eq. 5 in text; 10^{-4} $kgm^{-2}s^{-1}$; positive and negative values shaded are divergence and convergence, respectively) corresponding to the onset dates in (**a**, **d**) Region I [shown in Fig. 1a], (**b**, **e**) Region II [shown in Fig. 1b], and (**c**, **f**) Region III [shown in Fig. 1c]. The range of the onset date (in Julian Day) is shown on the top left, and the scale of the moisture flux vectors (in $kgm^{-1}s^{-1}$) is shown on the top right of each panel

is not yet established (Fig. 3a). Furthermore, at this time of onset over Region I, the cross-equatorial non-divergent moisture flux is limited to a narrow band of longitudes in east Africa (Fig. 3a). This changes to a wider expanse of the cross-equatorial moisture flux across the eastern tropical Indian Ocean from mid-May to mid-June, the period of onset over Region II with the southwesterly moisture flux established north of the equator and extending to parts of southern India (Fig. 3b). As the onset reaches Region III, the cross-equatorial non-divergent component of the moisture

flux spans over a larger longitude band (extending now east of 60°E) and the southwesterly moisture flux further broadens north of the equator, well into the Indian subcontinent by mid-June to mid-July (Fig. 3c). At this time of the evolution of the ISM, the non-divergent southwesterly moisture flux from across the Arabian Sea feeds into Regions I, II, and III (Fig. 3c). The corresponding precipitable water is also observed to progressively grow and expand over the subcontinental region as the onset date evolves from Region I to II and then to III (Fig. 3a-c).

The irrotational component of the vertically integrated (1000 to 200 hPa) moisture flux vectors shows them converging in Region I (Fig. 3d), Region II (Fig. 3e), and Region III (Fig. 3f) at the time of their onset dates. Interestingly, the strongest convergence of the irrotational moisture flux vectors is observed over the eastern equatorial Indian Ocean at time onset in Region I (Fig. 3d). This region of convergence of moisture flux is then observed to move progressively north over the southern Indian peninsula, the Gangetic Plains, and over southeast Asia as onset of ISM appears in Region II (Fig. 3b). At the time of the onset of ISM in Region III, the convergence shifts over the Indian subcontinent and spreads across northern parts of southeast Asia (Fig. 3d).

Similarly, the climatological mean of the non-divergent component of the vertically integrated (1000 to 200 hPa) moisture flux at the time of retreat dates for the three areas isolated in Fig. 1d-f are shown in Figs. S1a-c. Here, we note that the cross-equatorial moisture flux vectors continue over the eastern northern Indian Ocean (west of 60°E) and the southwesterly flux extend up to nearly ~ 15°N (Fig. S1a) but shift further southward (Fig. S1b) and is completely south of the Indian subcontinent (Fig. S1c) as the rainy season retreats over Areas I, II, and III, respectively. The cross-equatorial non-divergent component of the moisture flux also shrinks further to the west, successively, as the retreat progresses from Area I to II and then to III in Figs. S1a, b, and c, respectively. The precipitable water also concomitantly diminishes gradually as the monsoon retreats from Areas I, II, and III (Figs. S1a-c). Likewise, the irrotational component of the moisture flux indicates increased divergence of the moisture flux or a decreased moisture sink over Areas I, II, and III, as the rainy season retreated from these locations in Figs. S1d, e, and f, respectively. Notably, the convergence of irrotational moisture flux shows a distinct southward movement over Southeast Asia as the retreat progresses from Area I to II and then to III (Figs. S1d-f).

The commencement of the rainy season in Regions I, II, and III is marked by increases in γ_{ls} as noted in Fig. 4a. For instance, in all three regions, γ_{ls} reaches its highest value from the beginning of the year on the day of the onset over the three regions. Similarly, the retreat date of the rainy season is marked by the last day in the season, when γ_{ls} is the highest (Fig. 4b).

This change in the large-scale destabilization of the atmospheric column at the time of the onset of the rainy season is further investigated by examining the moisture flux components in the lower and middle troposphere. In Fig. 5a-c, the climatological non-divergent component of the vertically integrated (1000 − 700 hPa) moisture flux vectors and the precipitable water integrated from 1000 to 700 hPa show significant resemblance with the corresponding Fig. 3a-c. In other words, the column integrated moisture flux in Fig. 3a-c at the time of the onset over the three regions is dominated by the moisture transport and moisture content in the lower troposphere. Similarly, the lower tropospheric (1000 to 700 hPa) irrotational moisture flux vectors and moisture convergence in Fig. 5d-f is a near replica of the column-integrated irrotational moisture flux vectors with convergence exhibited in regions of onset. Initially, at the time of the onset over Region I, the moisture transport from Bay of Bengal appears to be significant, with some weak easterly flux from the west Pacific Ocean (Fig. 5a). However subsequently as the onset progresses to Regions II and III, the moisture transport from the Arabian Sea appears to be dominant and the easterly flux from the west Pacific disappears (Fig. 5b and c).

In contrast, the contribution of the middle troposphere (700 to 400 hPa) in the moisture transport at the time of the onset is significantly weaker (Fig. 6a-c). For instance, the southwesterly flux and the cross-equatorial non-divergent component of moisture flux in Fig. 6a-c are considerably weaker than their lower tropospheric counterparts in Fig. 5a-c. Furthermore, the moisture flux is more westerly north of 20°N in Fig. 6a-c, while the southerly component is more prominent in Fig. 5a-c. In Fig. 5a, when the southerlies are initially weak at lower troposphere, the middle troposphere experiences stronger dry westerlies engulfing the Regions I, III, the northern Arbian Sea and the northern Bay of Bengal (Fig. 6a). Subsequently, as the monsoon matures with onset over Regions II and III, the southwesterlies become strongest at lower levels and even reach deeper in the middle troposphere, expanding over the peninsular India (Figs. 5b and c and 6b and c). Simultaneously, the westerlies north of 20°N above 700 hPa weaken (Fig. 6b and c) as the monsoon trough establishes itself over eastern India. Interestingly, moisture accumulation is higher than ever over Region I and the Bay of Bengal, attributed to the deepening of moist southwesterlies, which ensures a more abundant moisture supply.

The mid-tropospheric irrotational moisture flux vectors in Fig. 6d-f shows a significant change from the corresponding lower tropospheric irrotational moisture flux vectors in Fig. 5d-f, with the former showing divergence relative to

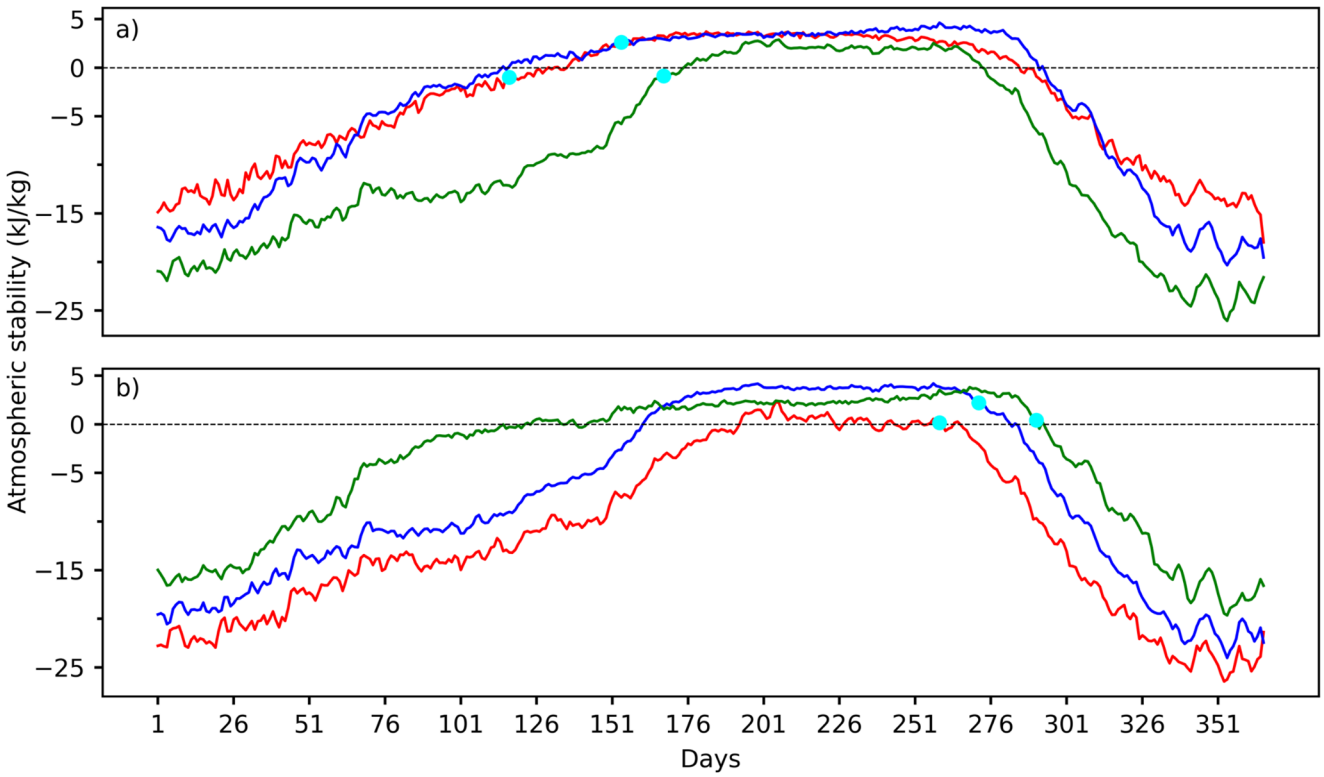

Fig. 4 (**a**) The climatological time series of the large-scale atmospheric stability (γ_{ls}; see text) averaged over Region I shaded in Fig. 1a (red line), Region II shaded in Fig. 1b (blue line), and Region III shaded in Fig. 1c (green line). The corresponding day of the onset of the rainy season is marked in each of the time series by a cyan-filled circle. (**b**) The climatological time series of γ_{ls} averaged over Area I shaded in Fig. 1e (red line), Area II shaded in Fig. 1f (blue line), and Area III shaded in Fig. 1g (green line). The corresponding day of the retreat of the rainy season is marked in each of the time series by a cyan-filled circle

convergence in the latter over the three regions of onset. In other words, in the layer between 700 and 400 hPa, there is a desiccation of moisture, as the moisture transport in the layer is unable to keep up with the condensation rate at the time of onset. Figures 3 and 5, and 6 confirm that the moisture source of the onset in the various regions is dominated by the lower tropospheric ($\leq$ 700 hPa) circulation and moisture gradients. Furthermore, the comparatively early onset over Region I is dictated by southerly moisture transport from the Bay of Bengal, while the onset over the rest of India is dominated by southwesterly transport from the Arabian Sea.

The retreat of the rainy seasons is also dominated by the changes in the lower tropospheric (1000 to 700 hPa) moisture flux with the southward migration of the southwesterly non-divergent moisture flux vectors as the retreat of the rainy season progresses from Area I (Fig. S2a), Area II (Fig. S2b), and Area III (Fig. S2c). Likewise, the precipitable water in the lower troposphere (Figs. S2a-c) resembles that of the column-integrated precipitable water in Figs. S1a-c suggesting the dominance of the lower tropospheric moisture content in the retreat of the rainy season. However, the southerly non-divergent moisture flux from the Bay of Bengal is persistent as the ISM retreats from Area III (Fig. S2c). In fact, cyclonic moisture transport is apparent, centered over eastern India-Bay of Bengal, suggesting the potential onset of the northeast monsoon. The easterly moisture flux from the western Pacific into Southeast Asia is also apparent in Figs. S2b and c. The irrotational moisture flux vectors and corresponding divergence of moisture flux in the lower troposphere (Figs. S2d-f) also show a close resemblance to their column-integrated counterparts in Figs. S1d-f with convergence of moisture reducing over the Indian subcontinent as the rainy season retreats from Areas I, II, and III. The southward shift of the convergence of the moisture flux over southeastern Asia as the retreat progresses from Area I to III is apparent in Figs. S2d-f.

In comparison, the mid-tropospheric moisture transport (Figs. S3a-c) is diminished in magnitude relative to the lower tropospheric moisture transport in Figs. S2a-c. However, the direction of the moisture transport over the Indian subcontinent is consistent with the corresponding irrotational moisture flux vectors in the lower troposphere (Fig. S2a-c). For instance, the gradual southward progression of the southwesterly flux and the persistent southerly flux in the Bay of Bengal, and the establishment of cyclonic

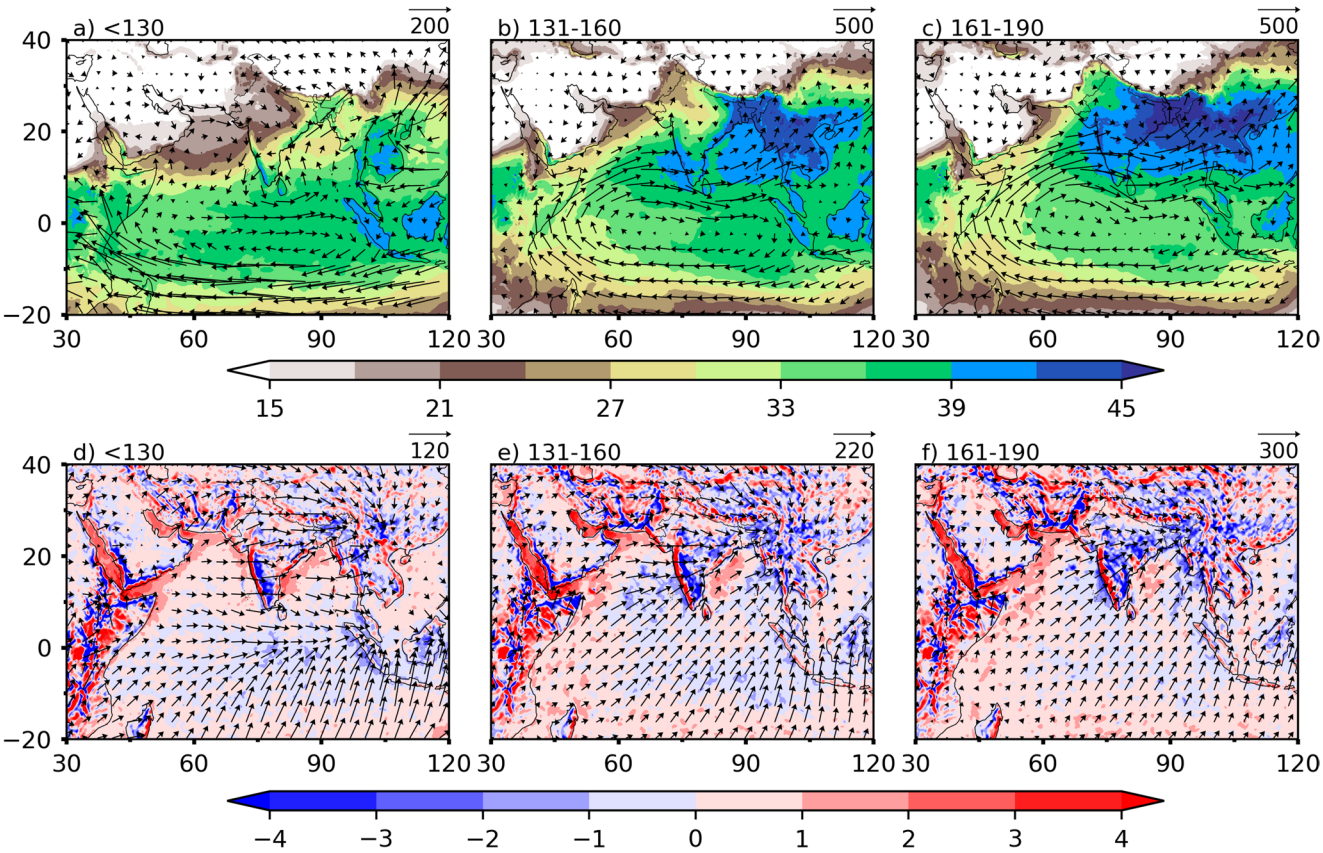

Fig. 5 The climatological mean of the (**a**, **b**, **c**) precipitable water (shaded; mm) non-divergent (Eq. 7 in text; vectors; $kgm^{-1}s^{-1}$) and (**d**, **e**, **f**) irrotational components of the vertically integrated (1000 to 700 hPa) moisture flux (Eq. 8 in text; vectors; $kgm^{-1}s^{-1}$) and divergence of moisture flux (Eq. 5 in text; 10^{-4} $kgm^{-2}s^{-1}$; positive and negative shaded values are divergence and convergence, respectively) corresponding to the onset dates in (**a**, **d**) Region I [shown in Fig. 1a], (**b**, **e**) Region II [shown in Fig. 1b], and (**c**, **f**) Region III [shown in Fig. 1c]. The range of the onset date (in Julian Day) is shown on the top left, and the scale of the moisture flux vectors (in $kgm^{-1}s^{-1}$) is shown on the top right of each panel

moisture transport in southeastern India and the Bay of Bengal in Figs. S3a-c is consistent with Figs. S2a-c. Even the establishment of the anticyclonic moisture flux over the east Asian monsoon region in Figs. S3a-c is consistent with the corresponding lower tropospheric moisture flux vectors in Figs. S2a-c. The irrotational moisture flux vectors and their divergence are considerably diminished in the mid-troposphere (Figs. S3d-f) compared to the lower troposphere (Figs. S2d-f) across the Indian subcontinent and southeast Asia. Therefore, at retreat, the moisture source is largely confined to the lower troposphere.

b) Interannual variability

The standard deviations of the onset date shown in Fig. 2a suggest that Regions I, II, and III exhibit a range of 10 to 15 days, 5 to 25 days, and 5 to 10 days, respectively. To understand these variations, we regress the onset date variability in these regions on the non-divergent component of the vertically integrated (1000 to 200 hPa) moisture flux vectors in Fig. 7a-c. The regression is computed by first detrending the time series at each grid point. Then, a least squares line is fitted, and its slope and corresponding *p*-values are obtained.

In Fig. 7a, the regressions suggest that early (later) onset over Region I is associated with a stronger (weaker) moisture transport from the western Indian Ocean across Southeast Asia, with an anomalous cyclonic (anticyclonic) moisture transport over the northern Bay of Bengal. Similarly, the early (later) onset of the rainy season over Region II is linked with a stronger (weaker) cross-equatorial moisture flux, a northward (southward) intrusion of the southwesterly moisture flux from the western Indian Ocean into peninsular India and across Bay of Bengal (Fig. 7b). Likewise, Fig. 7c shows that an earlier (later) onset of the rainy season in Region III is associated with a stronger (weaker) cross-equatorial anticyclonic (cyclonic) non-divergent moisture flux that nearly spans the latitudes just south of the equator to ~20°N and across southeast Asia. The regressions of the onset date variations of Region I on the precipitable water indicate a rise (fall) of the precipitable water over a broad area covering the Indian subcontinent and the

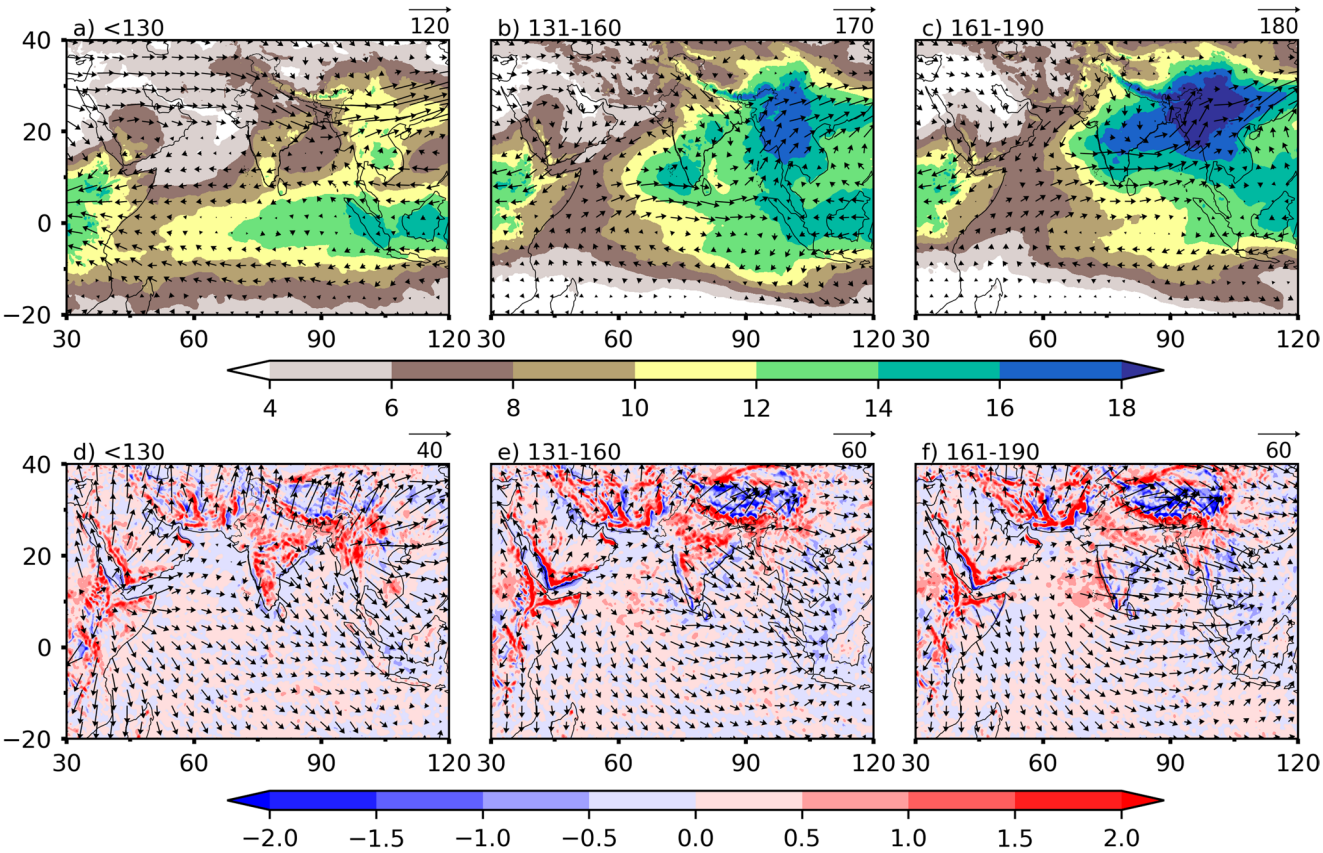

Fig. 6 The climatological mean of the (**a**, **b**, **c**) precipitable water (shaded; mm) non-divergent (Eq. 7 in text; vectors; $kgm^{-1}s^{-1}$) and (**d**, **e**, **f**) irrotational components of the vertically integrated (700 to 400 hPa) moisture flux (Eq. 8 in text; vectors; $kgm^{-1}s^{-1}$) and divergence (Eq. 5 in text; $10^{-4}\,kgm^{-2}s^{-1}$; positive and negative shaded values are divergence and convergence, respectively) corresponding to the onset dates in (**a**, **d**) Region I [shown in Fig. 1a], (**b**, **e**) Region II [shown in Fig. 1b], and (**c**, **f**) Region III [shown in Fig. 1c]. The range of the onset date (in Julian Day) is shown on the top left, and the scale of the moisture flux vectors (in $kgm^{-1}s^{-1}$) is shown on the top right of each panel

surrounding oceans in Fig. 7a, corresponding to early (late) onset. Likewise, Fig. 7b implies the rise (fall) of precipitable water over the northern Arabian Sea, northwestern, and northeastern India with an early (later) onset of the ISM over Region II. Similarly, Fig. 7c indicates the rise (fall) of precipitable water over northern India, with an early (later) onset of the rainy season over Region III. It should be noted that these regressions in Fig. 7a-c are like the corresponding anomalies of the moisture flux and precipitable water in the lower troposphere (Figs. S4a-c), suggesting their domination on the variability of the column-integrated anomalies of moisture. Furthermore, the modulation of the cross-equatorial moisture flux over the western Indian Ocean and southwesterly moisture flux along the Somali coast, with the onset date modulation in both Fig. 7a and S4a suggest the importance of monitoring the mass transport (especially in the lower troposphere) to anticipate variabilities of the ISM season as early as the onset of the rains in Region I.

Similarly, the regressions of the onset date variations on the irrotational vertically integrated (1000−200 hPa) moisture flux vectors indicate onset date variations in Region I are associated with anomalous irrotational moisture flux vectors emanating from the equatorial western Indian Ocean (Fig. 7d). Likewise, irrotational moisture flux vectors from equatorial central Indian Ocean are associated with onset date variations in Region II (Fig. 7e) and variations of the irrotational moisture flux vectors in the eastern equatorial Indian Ocean for onset date variations in Region III (Fig. 7f). We also observe that the regressions of the onset date variations with the irrotational moisture flux anomalies in the lower troposphere in Figs. S4d-f is nearly identical to the column-integrated anomalies in Fig. 7d-f. The lead-lag correlation at ±4 days around the onset date has also been computed for both the moisture flux components (for 1000−200 hPa only; Figs. S5-10), which shows a similar relationship as Fig. 7. This uniformity indicates that the moisture transport at the time of onset over the three regions is sustained before and after the onset of ISM.

The corresponding regressions of the retreat date variations on the non-divergent and irrotational components of

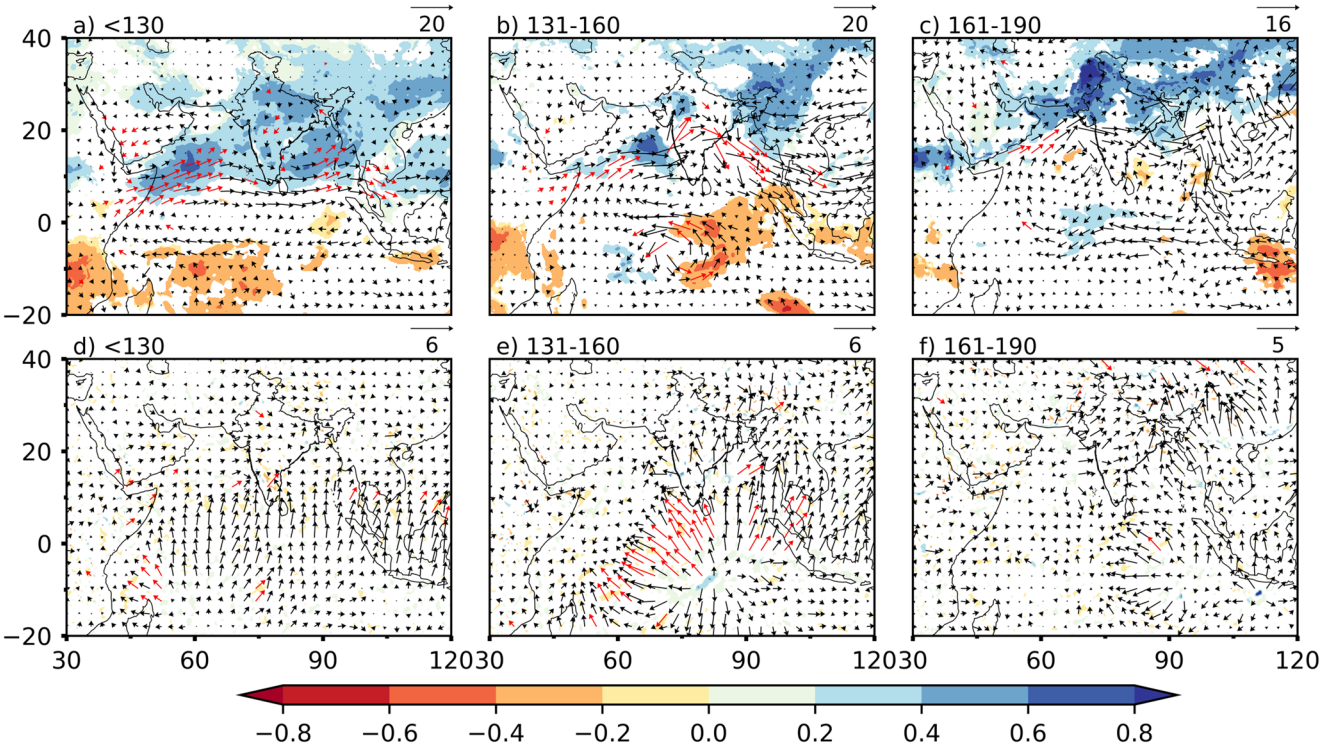

Fig. 7 The regression of the onset dates of (**a**, **d**) Region I [shown in Fig. 1a], (**b**, **e**) Region II [shown in Fig. 1b], (**c**, **f**) Region III [shown in Fig. 1c] on the (**a**, **b**, **c**) non-divergent components moisture flux vectors (unit: $kgm^{-1}s^{-1}day^{-1}$) and precipitable water (units: $mmday^{-1}$), and (**d**, **e**, **f**) irrotational components moisture flux vectors (unit: $kgm^{-1}s^{-1}day^{-1}$) and divergence (units: $kgm^{-2}s^{-1}day^{-1}$) vertically integrated for 1000–200 hPa. Significant values at 10% significance are shaded in colours and shown with red vectors. The range of the onset date (in Julian Day) is shown on the top left, and the scale of the slope of the moisture flux vectors (in $kgm^{-1}s^{-1}$) is shown on the top right of each panel

the moisture flux anomalies are shown in Fig. 8. Here, we observe that the early (later) retreat of the rainy season in Area I in Fig. 8a introduces easterly (westerly) moisture flux anomalies across the span of the domain. The retreat date variations in Area II show that the zonal moisture flux anomalies across the Indian subcontinent in Fig. 8b are slightly weaker compared to Fig. 8a, but the cross-equatorial flux is much stronger. Similarly, the retreat date variations in Area III show similar moisture flux anomalies (Fig. 8c) as in Area II, but with the cross-equatorial flux slightly more pronounced. The regressions of the retreat date variations on the precipitable water anomalies also indicate that early (later) retreat of the rainy season in these areas decreases (increases) the precipitable water anomalies in Areas I, II and III, as indicated by the shading in Fig. 8a-c. These flux anomalies are again dominated by the corresponding lower tropospheric moisture flux anomalies (Fig. S11a-c). As shown in Fig. 8, during ISM seasons of early retreat, the westerlies weaken rapidly, accompanied by a reduction in precipitable water. It is noteworthy that the cross-equatorial flux anomalies during the retreat phase are now directed towards the southern hemisphere, unlike the onset. This suggests weakening of monsoon westerlies with associated decrease in precipitable water anomalies, as evidenced by Fig. 8a-c.

The regressions of the retreat date variations on the irrotational moisture flux anomalies (Fig. 8d-f) indicate that early (later) retreat of the rainy season results in northerly (southerly) moisture flux anomalies across the domain (especially over the Bay of Bengal and Southeast Asia), suggesting an influx of drier (moist) air, respectively. These irrotational moisture flux anomalies are yet again dominated by the corresponding anomalies in the lower troposphere (Figs. S11d-f). The lead-lag correlations around the time of the retreat date (Figs. S12-17) show similar behaviour as in Fig. 8 for both non-divergent and irrotational components. This suggests that the moisture flux patterns at the time of retreat are sustained at least ± 4 days around the retreat date.

4 Conclusions

This study examines the evolution and variability of moisture flux over the seasonal cycle of the Indian summer monsoon (ISM) using modern atmospheric reanalysis (ERA5). The evolution of the ISM is featured through an objective

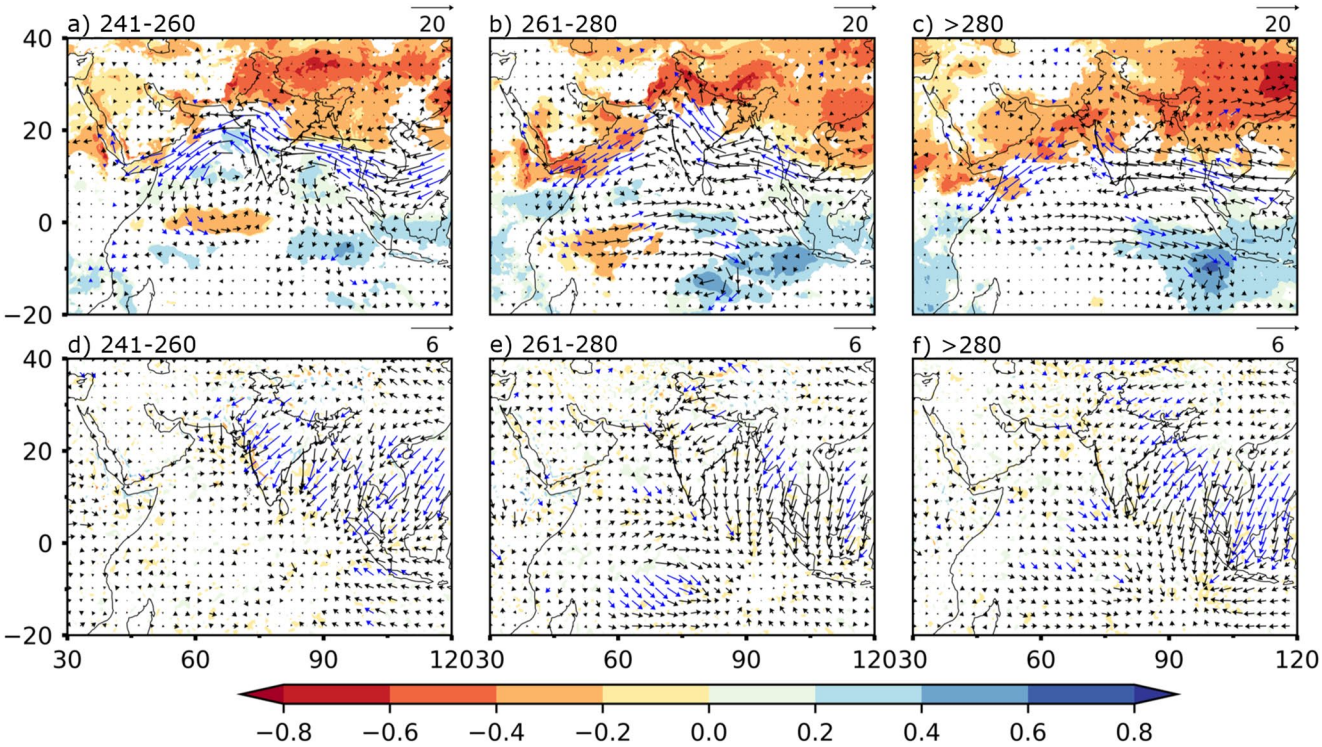

Fig. 8 The regression of the retreat dates of (**a**, **d**) Area I [shown in Fig. 1e], (**b**, **e**) Area II [shown in Fig. 1f], (**c**, **f**) Area III [shown in Fig. 1g] on the (**a**, **b**, **c**) non-divergent components moisture flux vectors (unit: $kgm^{-1}s^{-1}day^{-1}$) and precipitable water (units: $mmday^{-1}$), and (**d**, **e**, **f**) irrotational components moisture flux vectors (unit: $kgm^{-1}s^{-1}day^{-1}$) and divergence (units: $kgm^{-2}s^{-1}day^{-1}$) vertically integrated for 1000–200 hPa. Significant values at 10% significance are shaded in colours and shown with blue vectors. The range of the retreat date (in Julian Day) is shown on the top left, and the scale of the slope of the moisture flux vectors (in $kgm^{-1}s^{-1}$) is shown on the top right of each panel

criterion that pins the onset and retreat dates of the ISM to a calendar date (Misra et al., 2018; Noska and Misra 2016). Therefore, this study is novel in its approach to trace the evolution of the moisture flux vectors from ERA5 using this unique criterion for determining the onset and retreat dates of the ISM.

The onset and retreat dates of the ISM are defined at the granularity of the rainfall analysis (0.25° grid) as the first and the last day of the year when the daily rain rate exceeds the annual mean climatological rainfall at the grid point. Based on this definition, we isolate three spatially coherent regions of onset, with the earliest occurring over northeast India (Region I), followed by onset over Kerala-Karnataka-Gangetic-Brahmaputra basins (Region II), and then over central-northwestern India (Region III). Likewise, the retreat happens chronologically from northwestern (Area I), followed by central-northeastern (Area II), and finally over peninsular India (Area III).

The composite means of non-divergent moisture flux anomalies reveal that the onset of the ISM in Region I is sustained by moisture flux from the Bay of Bengal, while the cross-equatorial and southwesterly moisture flux is dominant in the onset of the ISM in Regions II and III. The subtle distinction between the onsets in Regions II and III is that there is a zonal broadening of the cross-equatorial and meridional broadening of the southwesterly moisture flux as the onset evolves from Regions II to III. Furthermore, the irrotational component of the moisture flux indicates comparatively strong convergence in the regions of onset. Similarly, the retreat displays a systematic southward withdrawal of the southwesterly moisture flux from Area I to II to III. Likewise, the precipitable water in the atmospheric column shows a systematic increase as the onset date evolves from Region I to III, while it decreases as it retreats from Area I to III. These changes in the moisture flux and precipitable water are dominated by changes in the lower troposphere (1000−700 hPa). The composites of the moisture flux vector for the homogeneous retreat date regions suggest an establishment of a cyclonic moisture flux centered over eastern India-Bay of Bengal, which indicates the onset of the northeast monsoons. In other words, the withdrawal of the ISM appears to be a competition between the moisture supply from the equatorial Indian Ocean in the form of cross-equatorial, southwesterly moisture flux and the continental drier air mass of the northeasterlies engulfing the region, corroborated by Deoras et al. (2024).

The interannual variations in the onset and retreat dates of the ISM indicate that the moisture transport associated with the cross-equatorial southwesterly moisture flux is significantly modulated. For example, an early (later) onset of the ISM over Regions I, II, and III suggests a strengthening (weakening) of the non-divergent southwesterly flux from the western Indian Ocean across the Bay of Bengal, respectively. Similarly, the early (later) retreat of the ISM over Areas I, II, and III indicates a more (less) weakening of the non-divergent southwesterly moisture flux across the two ocean basins, respectively. The irrotational component of the moisture flux anomalies shows comparatively less significant changes than the non-divergent component for onset date variations. However, for retreat date variations, the irrotational component of the moisture flux anomalies shows a larger contribution of drier northerly (moist southerly) moisture flux anomalies over the Bay of Bengal and Southeast Asia for early (late) retreat of ISM in Areas I, II, and III, respectively. These relationships seem to be sustained for at least ± 4 days around the onset/retreat dates.

This study provides an insight into the sources and sinks of moisture as the ISM evolves from a modern atmospheric reanalysis. The climatological variations and regression analysis done using ERA5 clearly suggest that the main source of the moisture transport critical to the onset and retreat of the ISM resides in the lower troposphere ($\leq$ 700 hPa). The insight gained from this work advocates monitoring of upper air variables in the southwesterly region of the Arabian Sea (along the Somali coast) and over the northeastern Bay of Bengal more actively to anticipate variations in the onset of the ISM rains, which consequently could be interpreted for seasonal anomalies of the ISM. This stems from the fact that earlier studies clearly indicate that the onset date variations of the ISM rainfall have a strong bearing on the following seasonal anomalies of the length of the ISM season and its seasonal rainfall anomalies (e.g., Bhardwaj & Misra, 2019; Misra and Bhardwaj 2020).

Our future work is to conduct a similar study with other global atmospheric analyses to acertain the uncertainties in the moisture sources and sinks. Furthermore, we also wish to carry out this analysis over a much longer period using, for example, the centennial reanalysis products to understand the variations of the moisture flux of the ISM evolution at low-frequency timescales beyond the interannual timescales.

Supplementary Information The online version contains supplementary material available at https://doi.org/10.1007/s00703-025-01112-9.

Acknowledgements Amarjeet acknowledges the Fulbright-Kalam Climate Doctoral Program, sponsored by the United States-India Educational Foundation (USIEF), for providing fellowship (Award no. 3015/FKDR/2024–2025) to conduct research at Florida State University, USA. He also acknowledges the DST-INSPIRE fellowship (IF190627) provided by the Department of Science and Technology, Government of India, to conduct research at IIT Kharagpur, India. AC gratefully acknowledges the financial support given by the Indian Institute of Tropical Meteorology, Ministry of Earth Sciences, Government of India (Ref. No. 11TM/MM-111/2024/A1-P06/SO-006) to conduct research under Monsoon Mission-III. AKG thanks the Anusandhan National Research Foundation (ANRF), New Delhi, for financial support under the J.C. Bose Fellowship (Grant no. JBR/2021/000019). We acknowledge the anonymous reviewers for providing their valuable suggestions, which enhance the quality of the manuscript.

Author contributions Amarjeet is involved in conceptualization, methodology, software, validation, formal analysis, investigation, resources, data curation, writing—review, editing and visualization. VM is involved in conceptualization, investigation, writing—original draft, review, editing, and supervision. AC and AKG contributed to writing—review, editing, and supervision.

Funding No funding sources have been used in this study.

Data availability The ERA5 reanalysis data is taken from (ERA5, 2022). The IMD data is obtained from https://www.imdpune.gov.in/cmpg/Griddata/Rainfall_25_NetCDF.html. We used Python software to generate figures. The data can be provided on a reasonable request to the corresponding author.

Declarations

Conflict of interest The authors declare no conflict of interest in this study.

References

Amarjeet, Misra V, Chakraborty A, Gupta AK, Sharma V (2025) A Study of Recent Changes in Moisture Flux Patterns Over India: Implications for Indian Summer Monsoon Rainfall. Int J Climatol. https://doi.org/10.1002/joc.8927

Amarjeet, Sharma V, Pandey CP, Gupta AK, Chakraborty A (2023) Study of moisture flux over Uttarakhand state: signature of cloudbursts. Clim Dyn 61:5349–5366

Ananthakrishnan R, Soman MK (1988) The onset of south-west monsoon over kerala: 1901–1980. J Climatol 8(3):283–296

Ananthakrishnan R, Acharya UR, Rama Krishnan AR (1967) On the criteria for declaring the onset of the southwest monsoon over Kerala. Forecasting Manual, FMU Rep. IV-18.1, India Meteorological Department, Pune, India, 52 pp

Bhardwaj A, Misra V (2019) Monitoring the Indian Summer Monsoon Evolution at the Granularity of the Indian Meteorological Sub-divisions using Remotely Sensed Rainfall Products. Remote Sensing, 11(9):1080. https://doi.org/10.3390/rs11091080

Chakraborty A, Behera SK, Mujumdar M, Ohba R, Yamagata T (2006) Diagnosis of tropospheric moisture over Saudi Arabia and influences of IOD and ENSO. Mon Weather Rev 134:598–617

Clemens SC, Oglesby RJ (1992) Interhemispheric moisture transport in the Indian ocean summer monsoon: data-model and model-model comparisons. Paleoceanography 7(5):633–643

Cook BI, Seager R (2013) The response of the North American monsoon to increased greenhouse gas forcing. J Geophys Res Atmos 118:1690–1699. https://doi.org/10.1002/jgrd.50111

Das S, Goswami DJ, Mahanta R, Saha P, Goswami BN (2024) Dynamics of May 'onset' of Indian summer monsoon over Northeast India. Q J R Meteorol Soc 150(764):4533–4549

Deoras A, Turner AG, Volonté A, Menon A (2024) The role of mid-latitude dry air during the withdrawal of the Indian summer monsoon. Q J R Meteorol Soc 150(765):5094–5112

ERA5 (2022) : https://www.ecmwf.int/en/forecasts/datasets/reanalysis-datasets/era5

Fasullo J, Webster PJ (2003) A hydrological definition of Indian monsoon onset and withdrawal. J Clim16:3200–3211.

Ghosh SK, Pant MC, Dewan BN (1978) Influence of the Arabian sea on the Indian summer monsoon. Tellus 30:117–125

Hersbach H, Bell W, Berrisford P, Horanyi A, Sabater JM, Nicolas J et al (2019) The ERA5 global reanalysis. Q J R Meteorol Soc 146:1999–2049

Janowiak JE, Xie P (2003) A global-scale examination of monsoon-related precipitation. J Clim 16:4121–4133

Khairoutdinov M, Randall D (2006) High-resolution simulation of shallow-to-deep convection transition over land. J Atmos Sci 63(12):3421–3436. https://doi.org/10.1175/JAS3810.1

Krishnakumar V, Lau KM (1998) Possible role of symmetric instability in the onset and abrupt transition of the Asian monsoon. J Meteorol Soc Japan Ser II 76(3):363–383

Krishnamurti TN, Ardanuy P, Ramanathan Y, Pasch R (1981) On the onset vortex of the summer monsoon. Mon Weather Rev 109(2):344–363

Krishnamurti TN, Bedi HS, Hardiker V, Watson-Ramaswamy L (2006) An Introduction to Global Spectral Modeling. Oxford University Press, Springer, New York, p 320. https://doi.org/10.1007/0-387-32962-5

Levine RC, Turner AG (2011) Dependence of Indian monsoon rainfall on moisture fluxes across the Arabian sea and the impact of coupled model sea surface temperature biases. Clim Dyn 38:2167–2190

Misra V, Bhardwaj A (2020) The impact of varying seasonal lengths of the rainy seasons of India on its teleconnections with tropical sea surface temperatures. Atmos Sci Lett 21(3):e959 https://doi.org/10.1002/asl.959

Misra V, Pantina P, Chan C, S., DiNapoli S (2012) A comparative study of the Indian summer monsoon hydroclimate and its variations in three reanalyses. Clim Dyn 39:1149–1168. https://doi.org/10.1007/s00382-012-1319-y

Misra V, Bhardwaj A, Mishra A (2018) Local onset and demise of the Indian summer monsoon. Clim Dyn 51:1609–1622

Noska R, Misra V (2016) Characterizing the onset and demise of the Indian summer monsoon. Geophys Res Lett 43(9):4547–4554. https://doi.org/10.1002/2016GL068409

Pai DS, Rajeevan M, Sreejith OP, Mukhopadhyay B, Satbha NS (2014) Development of a new high spatial resolution (0.25 × 0.25) long period (1901–2010) daily gridded rainfall data set over India and its comparison with existing data sets over the region. Mausam 65(1):1–18

Pai DS, Sridhar L, Badwaik MR, Rajeevan M (2015) Analysis of the daily rainfall events over India using a new long period (1901–2010) high resolution (0.25× 0.25) gridded rainfall data set. Clim Dyn 45:755–776. https://doi.org/10.1007/s00382-014-2307-1

Pathak A, Ghosh S, Martinez JA, Dominguez F, Kumar P (2017) Role of oceanic and land moisture sources and transport in the seasonal and interannual variability of summer monsoon in India. J Clim 30(5):1839–1859

Patil C, Prabhakaran T, Ray S, K.C. and, Karipot A (2019) Revisiting moisture transport during the Indian summer monsoon using the moisture river concept. Pure Appl Geophys 176:5107–5123

Pisharoty PR (1965) Evaporation from the Arabian Sea and the Indian southwest monsoon. In Proc. Sym. Met., Results of IIOE, Bombay. (Available from IMD, New Delhi). pp. 43–45

Prasad VS, Hayashi T (2005) Onset and withdrawal of Indian summer monsoon. Geophys Res Lett 32(20):L20715. https://doi.org/10.1029/2005GL023269

Ramage C (1971) Monsoon Meteorology, Int. Geophys. Ser, vol 15. pp., Academic, San Diego, California, p 296

Ratna SB, Cherchi A, Joseph PV (2016) Moisture variability over the Indo-Pacific region and its influence on the Indian summer monsoon rainfall. Clim Dyn 46:949. https://doi.org/10.1007/s00382-015-2624-z

Rosen RD, Salstein DA, Peixoto J (1979) Streamfunction analysis of interannual variability in large-scale water vapor flux. Mon Weather Rev 107(12):1682–1684

Saha P, Mahanta R, Goswami BN (2023) Present and future of the South Asian summer monsoon's rainy season over Northeast India. npj Climate and Atmospheric Science 6(1):170

Sebastian DE, Pathak A, Ghosh S (2016) Use of atmospheric budget to reduce uncertainty in estimated water availability over South Asia from different reanalyses. Sci Rep 6(1):29664

Shah R, Mishra V (2014) Evaluation of the reanalysis products for the monsoon season droughts in India. J Hydrometeorol 15(4):1575–1591

Sharma D, Das S, Goswami BN (2023) Variability and predictability of the Northeast India summer monsoon rainfall. Int J Climatol 43(11):5248–5268

Sharma V, Amarjeet, Sharma S, Chakraborty A (2024) Evidence of strengthening of tropical Easterly jet after 1998 climate shift using ERA-5 datasets. Theoret Appl Climatol 155:5859–5874

Sharma V, Amarjeet, Singh GP, Chakraborty A (2025) Variabilities in onset and withdrawal characteristics of Indian summer monsoon after 1998 climate shift: dynamical role of Somali jet. Theoret Appl Climatol 156(10):1–14

Syroka J, Toumi R (2004) On the withdrawal of the Indian summer monsoon. Q J Royal Meteorological Society: J Atmospheric Sci Appl Meteorol Phys Oceanogr 130(598):989–1008

Trenberth KE, Dai A, Rasmussen RM, Parsons DB (2003) The changing character of precipitation. Bull Am Meteorol Soc 84(9):1205–1218

Volonté A, Turner AG, Menon A (2020) Airmass analysis of the processes driving the progression of the Indian summer monsoon. Q J R Meteorol Soc 146(731):2949–2980

Yadav RK, Singh BB (2017) North equatorial Indian ocean convection and Indian summer monsoon June progression: a case study of 2013 and 2014. Pure Appl Geophys 174:477–489. https://doi.org/10.1007/s00024-016-1341-9

Yanai M, Li C, Song Z (1992) Seasonal heating of the Tibetan plateau and its effects on the evolution of the Asian summer monsoon. J Meteorol Soc Japan Ser II 70(1B):319–351

Zahan Y, Mahanta R, Rajesh PV, Goswami BN (2021) Impact of climate change on North-East India (NEI) summer monsoon rainfall. Clim Change 164:1–19

Zeng X, Lu E (2004) Globally unified monsoon onset and retreat indexes. J Clim 17(11):2241–2248. https://doi.org/10.1175/1520-0442(2004)0172.0.CO;2